Localization of multiple acoustic sources in the shallow ocean

Tracianne B. Neilsen[a)]
Applied Research Laboratories, The University of Texas at Austin, Austin, Texas 78713-8029

(Received 12 October 2004; revised 20 June 2005; accepted 1 August 2005)

An iterative, rotated coordinates inversion technique is applied in conjunction with spatial narrowband filters in matrix form to localize multiple acoustic sources in the shallow ocean. When the iterative, rotated coordinates inversion technique is applied to broadband horizontal line array data designed to simulate a group of moving ships, the bearing of the loudest source is quickly identified. Both passband and stop band matrix filters are constructed for an angular sector centered on the identified bearing. Data filtered with the passband filters are used in the inversion to obtain estimates of the remaining source parameters, range, depth, course angle and speed, and prominent environmental parameters. Additional inversions applied to data modified by the stop band filters yield the bearing of the next loudest source. The procedure is repeated until all detectable sources have been localized. Results of applying this strategy to several simulated cases are presented.
 [DOI: 10.1121/1.2041307]

PACS number(s): 43.30.Wi, 43.30.Pc [WLS] Pages: 2944–2953

I. INTRODUCTION

A central goal in many areas of underwater acoustics research is the localization of acoustic sources. Traditionally, the first task is to identify the number of sources and their bearings. Next, the ranges from the receiver array to the sources are estimated. In contrast, the goals of the present work are to find the locations and trajectories of multiple acoustic source without *a priori* knowledge of the number of sources present by applying an optimization algorithm[1,2] and narrowband matrix filters[3] to broadband horizontal line array (HLA) data.

Identification of the bearing of an acoustic source can be accomplished with many techniques. A large number of these methods are based on beamforming, in which the responses of the array for sound received from multiple bearing angles, referred to as look-directions, are compared to plane-wave replica vectors: the response expected on the array for a plane-wave arrival from a source in the far-field at that bearing. A detailed description of beamforming can be found in Ref. 4. For the present, the relevant point is that while advanced beamforming techniques accurately identify source bearings in a wide variety of cases, they must be used in conjunction with other algorithms to obtain source ranges and trajectories.

Another set of techniques developed for source localization are referred to as matched field processing (MFP) algorithms. In contrast to plane-wave beamforming, the array response in each look-direction is compared, in MFP, to the replica vectors calculated when the effects of the ocean environment on the plane-wave propagation are included. Thus, the replica vectors depend inherently on the assumed environmental properties. When the environment is well known, MFP can yield good values for source locations in bearing, range, and depth.[5–7] But if the assumed environmental characteristics are incorrect, a case referred to as environmental mismatch, the accuracy of MFP decreases.

To tackle the problems of environmental mismatch, a number of match-field inversion methods,[8] also known as geoacoustic inversions, have emerged. The goal of these optimizations is to obtain accurate estimates for the environmental properties of the shallow-ocean. References 9 and 10 contain reports of benchmark workshops in which such inversion algorithms are applied to synthetic data for range-independent and range-dependent environments, respectively. The articles therein illustrate the wide variety of optimizations currently in use.

A few geoacoustic optimization algorithms have been adapted to invert for the location of a single source along with the environmental parameters. For example, in Refs. 11–13, range and depth of the source are found along with environmental parameters. In Ref. 1, estimates of bearing, range, depth, course angle, and speed of a moving source, as well as environmental characteristics, are found for broadband, HLA data designed to simulate a moving source. The *posteriori* distributions in Ref. 11 and the rotated coordinates in Ref. 1 confirm that the acoustic field is much more sensitive to changes in the source parameters than changes in the environmental properties, as described in Ref. 14.

Building on the work in Refs. 1 and 2, the iterative, rotated coordinates inversion method is applied herein in conjunction with spatial, narrowband filters in matrix form[3] to synthetic, broadband, HLA data generated for multiple, moving, acoustic sources. With no *a priori* knowledge about the number of sources present, the inherently single-source inversion quickly identifies the bearing of the strongest source. Two kinds of narrowband matrix filters are then designed about the identified angle. First, passband matrix filters[3] are constructed to isolate sound originating from an angular sector about the source bearing and are applied to the original data. The resulting filtered data set is used in the inversion to obtain estimates of the source's range, depth, and trajectory. Second, stop band matrix filters remove sound

[a)]Electronic mail: neilsen@arlut.utexas.edu

corresponding to sources in an angular sector about the identified bearing. The resulting modified data are basically equivalent to broadband, HLA data from one less source than the original data. Application of the inversion technique to the modified data yields the bearing of the next strongest source. New sets of matrix filters are created, and the process is repeated until all detectable sources have been localized.

Details and examples of applying this iterative invert-and-filter technique are presented in this paper, which is organized as follows. Section II describes the inversion technique and the procedure for constructing the matrix filters. The performance of the iterative invert-and-filter strategy is demonstrated in Sec. III, for cases of two, four, and ten moving sources. Gaussian noise is added to the ten-source case. The case of environmental mismatch is explored in Sec. III D. Section IV contains conclusions that have been obtained thus far and further potential applications of these techniques.

II. METHODOLOGY

Brief overviews of the inversion method and the matrix filters are presented. Further details about the techniques are available in Refs. 1–3. All computations use complex spectral values at multiple frequencies obtained when a fast Fourier transform (FFT) is performed on time series received on an array of hydrophones.

A. Iterative inversion method

Inversion methods are characterized by three main components: the forward model, the cost function to be minimized, and the search algorithm. For the work presented in this paper, a range-independent, normal mode model, ORCA,[15] is used to produce the modeled field. The modeled field is compared to the data in a cost function based on a cross-phone correlation that is summed coherently over both frequencies and time (range) sequences. The search algorithm is the iterative inversion method referred to as systematic decoupling using rotated coordinates (SDRC),[1,2] which uses multiple sets of rotated coordinates in a series of fast simulated annealing optimizations.

1. Cost function

The cost function minimized in our analysis, based on the coherent, broadband correlation first introduced in Ref. 6, is defined as

$$E(\mathbf{x}) = 1 - \frac{1}{n}\sum_{t} C_1(\mathbf{x},t), \tag{1}$$

where n is the number of time sequences. $C_1(\mathbf{x},t)$ is the coherent, broadband, cross-phone correlation between data and model, at time sequence t, for the set of physical parameters $\mathbf{x}$:

$$C_1(\mathbf{x},\mathbf{t}) = \sum_{f}\sum_{j}\sum_{i>j} D_i(f,t)D_j^*(f,t)M_i^*(f,t,\mathbf{x})M_j(f,t,\mathbf{x}), \tag{2}$$

with i and j indicating the receivers. $D_i(f,t)$ is the measured spectra on the ith hydrophone at frequency f and is normalized at each time t such that

$$\sqrt{\sum_{f}\sum_{j}\sum_{i>j} |D_i(f,t)D_j^*(f,t)|^2} = 1. \tag{3}$$

A single set of source parameters and environmental parameters in $\mathbf{x}$ are used to calculate the modeled spectral values $M_i(f,t,\mathbf{x})$ (complex pressure field), which are normalized in the same manner. In the examples, the data $\mathbf{D}$ are produced by multiple sources, but the modeled values $\mathbf{M}$ are generated assuming only a single source.

2. The SDRC algorithm

The cost function E is minimized by a series of fast simulated annealing optimizations in a process called SDRC. The SDRC approach developed in Refs. 1 and 2 is designed to quickly identify the most sensitive parameters, defined as those which have the largest influence on the cost function, without *a priori* decisions regarding which parameters are not to be varied during the optimization.

The SDRC method uses rotated coordinates, introduced in Ref. 16, to navigate the parameter search space because often there is a correlation between how various parameters influence the cost function E. The application of rotated coordinates transforms the inversion problem from the N physical parameters in $\mathbf{x}$ to a coordinate system that is better aligned with the prominent valleys and gradients of the search space. The transformation is accomplished via diagonalizing $\mathbf{K}$, the covariance matrix of the cost function gradients. The components of $\mathbf{K}$ are defined by

$$K_{ij} = \int_{\Omega} \frac{\partial E}{\partial \hat{x}_i}\frac{\partial E}{\partial \hat{x}_j} d\Omega, \tag{4}$$

and $i,j=1,\ldots,N$. The integration is performed over the N-dimensional volume Ω using an efficient Monte Carlo algorithm.[17] The values of $\hat{\mathbf{x}}$ are dimensionless: the dimensions have been removed from the physical parameters by dividing them by the difference between the respective maximum and minimum values of the parameters in the volume Ω.

An eigenvalue decomposition of $\mathbf{K}$ yields eigenvectors $\mathbf{v_i}$ and eigenvalues s_i. The eigenvectors $\mathbf{v_i}$, which are referred to as the rotated coordinates, indicate how the parameters are coupled, and are used in constructing the explicit expression for the parameter perturbations in the fast simulated annealing optimization.[16,18] Specifically, at each step in the inversion, a single eigenvector $\mathbf{v_j}$ is used to change the set of parameters in $\hat{\mathbf{x}}$ to the new values $\hat{\mathbf{x}}'$ by

$$\hat{\mathbf{x}}' = \hat{\mathbf{x}} + \tfrac{1}{2}\gamma^3\mathbf{v_j}, \tag{5}$$

where γ is randomly selected from the interval $(-1,1)$. Equation (5) is chosen because it tends toward small perturbations but allows large perturbations and works well with

the fast simulated annealing algorithm.[16,18] The eigenvalues s_i indicate which rotated coordinates or, equivalently, which combinations of parameters, have the largest effect on the cost function. Both the parameter couplings and the relative sensitivities depend on Ω, the bounds on the integration in Eq. (4).

Although the use of rotated coordinates, as compared to standard coordinates, in the annealing increases the efficiency of the optimization, it is, nevertheless, extremely difficult to obtain reliable estimates for a large number of parameters from a single inversion in which all the rotated coordinates are varied; the difficulty arises from the wide range of the cost function's sensitivities to changes in the different parameters. The SDRC method[1] has been designed to take advantage of the diverse sensitivities and to find estimates for the most sensitive parameters first before trying to obtain the less sensitive parameters. In SDRC multiple sets of rotated coordinates, each corresponding to a subsequently smaller set of parameter bounds, are used in a series of inversions. For each annealing, only the primary rotated coordinates, defined as those with large corresponding eigenvalues, are used to vary the parameters as in Eq. (5). As the most sensitive parameters become better defined and the bounds on these parameters in the volume Ω are reduced as described in Ref. 2, subsequent sets of primary rotated coordinates change and different parameters are varied more substantially. It is important to note that throughout the iterative algorithm the bounds on the annealing search space are not changed.

B. Spatial filters

Once an approximate source bearing is obtained, narrowband, spatial filters in matrix form, centered on the estimated source bearing, are computed for the frequencies of interest: $f_1, \ldots, f_P$. Matrix filters were originally developed as frequency selective filters for short time series[19] and have been employed for source localization in passive SONAR problems.[20] Many design algorithms are computationally expensive and are not practical in situations where new matrix filters may have to be created and used in real time. The matrix filters applied in the present work are constructed with an efficient method based on the solution of a set of least-squares (LS) problems.[3]

For an array with N_e elements the filtering operation is the matrix-vector product $\mathbf{GD}$, where the $N_e \times N_e$ matrix filter $\mathbf{G}$ is complex, non-Hermitian, rank-deficient, and a function of both the angular window W and frequency f.

The filter design requires the construction of a matrix of steering vectors $\mathbf{Y}(f)$ whose columns are the plane-wave replica vectors. Each replica vector $\mathbf{y_i}(f)$ is an N_e vector giving the plane-wave, array element response due to a single far-field source at angle ϕ_i.

The response of the matrix filter $\mathbf{G}$, for a given frequency f, is given by

$$\mathbf{G}y_i = \ell_i y_i, \quad i = 1, \ldots, M, \tag{6}$$

where M is the number of discrete angles $\{\phi_i, \ldots, \phi_M\}$ covering the bearing space. In the applications presented here, $\ell_k \in \{0,1\}$. For a spatial passband filter about the angular window $W=[\phi_i, \phi_j]$, $\ell_k=1$, for $i \leqslant k \leqslant j$, and $\ell_k=0$, otherwise. Similarly, for the spatial stop band filter, $\ell_k=0$, for $i \leqslant k \leqslant j$, and $\ell_k=1$, otherwise. By defining $\mathbf{\Lambda} = \mathrm{diag}(\ell_1, \ldots, \ell_M)$, the M equations in Eq. (6) can be written as $\mathbf{GY}=\mathbf{Y\Lambda}$. This leads to the rank-deficient least-squares problem:

$$\min_{g_{ij}} \|\mathbf{GY} - \mathbf{Y\Lambda}\|^2 = \min_{g_{ij}} \|\mathbf{Y}^H\mathbf{G}^H - \mathbf{\Lambda}^H\mathbf{Y}^H\|^2, \tag{7}$$

where the superscript H denotes conjugate transpose. A standard numerical method for the solution of rank-deficient linear LS problems[21] based on calculating the psuedo-inverse $\mathbf{P}=(\mathbf{Y}^H)^{+}$[17] is used such that the solution to Eq. (7) is

$$\mathbf{G} = \mathbf{Y\Lambda P}^H. \tag{8}$$

The computation of the matrix filters $\mathbf{G}$, as a function of the angular window W and the frequency f, is efficient enough for practical applications because (1) the replica vectors Y and corresponding pseudo-inverses P for frequencies and angles of interest can be calculated once and stored, and (2) the filtering operation can be calculated with only a few vector inner products instead of a full matrix-vector product because of the low rank of the filters.

Studies by Stotts[22] have shown that optimum matrix filters can be designed if the array configuration is taken into account when choosing the rank of the psuedo-inverse. This work has proven useful, especially for nonuniform arrays.[23] In the present work, however, the array elements are uniformly spaced and a standard threshold is used.

III. EXAMPLES

Examples are presented to show how multiple applications of the SDRC inversion method and the matrix filters on broadband, HLA data can locate and track multiple sources in an uncertain ocean environment. The iterative invert-and-filter strategy proceeds as follows. First, a SDRC inversion is performed with the broadband, HLA data. The inversion algorithm computes the modeled field $M_j(f,t,\mathbf{x})$ in Eq. (2) based on a single set of source parameters in $\mathbf{x}$. The source bearing found by the inversion, θ_1, is the initial bearing of the source with the loudest received level on the HLA. Stop band filters, also referred to as notch filters, are constructed about θ_1 and applied to the original data to effectively remove the contribution of the loudest source in the element-level data. The resulting filtered data are processed in the inversion to obtain the bearing of the next loudest source, θ_2. A new set of notch filters is created about θ_2 and applied to the data. The process is repeated until all discernible source bearings are found. In parallel to this source-bearing identification and source-removal procedure, passband filters are constructed about each angle θ_i that is identified as an initial source bearing. Data filtered with passband filters contain sound originating in the designated angular sector, which ideally contains only one source. These filtered data sets, one for each θ_i, can be used in a SDRC inversion to find additional source parameters, depth z_s, range r_0, course angle ϕ, and speed v, as well as environmental characteristics.

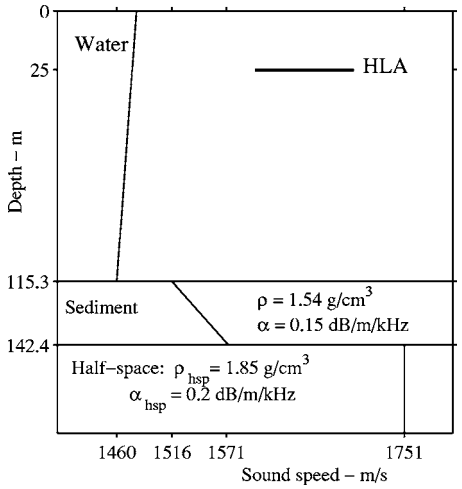

FIG. 1. Shallow ocean environment for the examples in Sec. III. The bold, horizontal line represents the HLA at a depth of 25 m. The other bold, solid lines show the sound speed c in the water, sediment, and half-space. The density ρ and the attenuation α in the sediment and the half-space are specified.

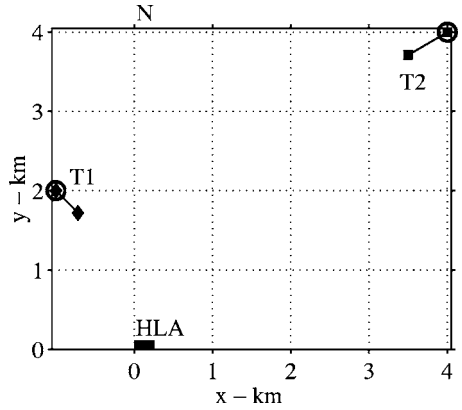

FIG. 2. Geometry of the sources and receivers for the example in Sec. III A. The initial locations are shown as circles and the final as a diamond for T1 and a square for T2. The horizontal aperture covered by the array is illustrated as a box on the x axis.

Some of the questions that arise when considering the above strategy include the following. (1) Is there a ratio of source levels for which the bearing θ_i found by the inversion does not correspond to an actual source bearing? (2) How many sources can be identified by successive applications of the inversions and matrix filters? (3) In what cases is the invert-and-filter scheme unable to locate sources? (4) What influence does an incorrect description for the ocean environment have on the estimates of the source parameters obtained by the inversion? (5) Can estimates of the environmental characteristics be identified while applying the SDRC inversion method to data filtered to isolate a loud source? Three test cases are used to explore these questions.

The data for the test cases are generated in the following manner. First, ORCA[15] is used to obtain the broadband modal eigenvalues for the specified environment. These modal eigenvalues are combined with the individual, unique source spectra, broadband source level, initial location, and trajectory for each source to generate the acoustic field received at the array. The resulting data file contains the FFT of the time series produced by the designated moving sources in the specified environment. For the ten-source case, noise is added to the acoustic field.

The environment and array specifications are the same for all cases. The environment is based on one of the test cases from the 1997 Geoacoustic Inversion Workshop,[9] illustrated in Fig. 1. The HLA is located at a depth of 25 m and consists of 65 elements that are spaced 4 m apart for a total horizontal aperture of 256 m.

A. Two sources with varying source levels

Multisource field data from two sources are simulated with different ratios of the source levels to explore (1) whether or not the inherently single-source SDRC inversion algorithm can reliably obtain a valid source bearing when applied to the field from two sources and (2) if an ambiguous source bearing is found when the sound received on the array from two sources is approximately equivalent. Specifically, the complex spectra from two, concurrent sources at 41 evenly spaced frequencies from 50 to 250 Hz received on the HLA at eleven time sequences that cover a 3-min time interval are generated with different source levels. The positions of the two sources during the 3 min and the HLA are illustrated in Fig. 2. Table I lists the sources' characteristics.

In this example, the SDRC inversion method is applied to data generated for different ratios of the broadband source levels of T1 and T2, and the bearing obtained by the inversion always matches one of the correct source bearings. The broadband source level is the total intensity of the source integrated over the specified frequency band. The source level of T2 is held at 140 dB, while the source level of T1 is varied from 105 to 130 dB. For cases when the source level of T1 is less than 123 dB, the inversion properly identifies an initial bearing of $45° \pm 0.5°$, the bearing of T2. In addition, good estimates are obtained for the range r (within 200 m), the course angle ϕ (within 4°), and the speed v (within 0.3 m/s) by inversions performed starting with several different sets of initial source parameters and with the parameter bounds on the inversions listed in Table I. When the source level of T1 is greater than 125 dB, the initial bearing of T1 is found within 0.3°, and r, ϕ, and v are found with the same accuracy as cited earlier. When the T1 source level is 123 dB, the initial bearing of T2 is found, and good estimates of r, ϕ, and v are obtained from about half of the inversions. Similarly, inversions based on data with a T1

TABLE I. Characteristics of the two sources (T1 and T2) for the synthetic data described in Sec. III A: the source depth z_s, the initial range r_0 and initial bearing θ from the array, the course angle ϕ, the speed v. All angles are measured relative to North (0°). The last two columns list the bounds on the parameters for the inversions.

Parameters	T1	T2	Min	Max
z_s (m)	40	6	1	70
r_0 (km)	2.236	5.657	0.1	10
θ (deg)	−26.6	45	−90	90
ϕ (deg)	135	240	0	360
v (m/s)	2.2	3.2	1	10

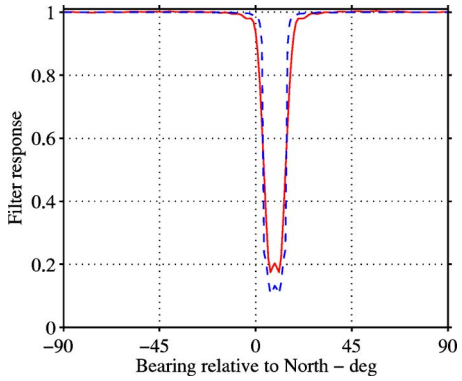

FIG. 3. A 10° notch filter about 11° at 50 Hz (dashed line) and 250 Hz (solid line) for the environment and array in Fig. 1.

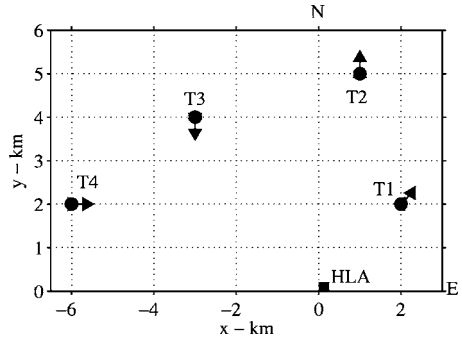

FIG. 4. Source configuration for examples in Sec. III B. The circles denote the starting location, and the arrows indicate the source positions 3 min later. The rectangle near the origin shows the horizontal aperture covered by the HLA.

source level of 125 dB find the initial bearing of T1 reliably and sometimes find good estimates for the other source parameters. For a source level of 124 dB, the sources have the same received level on the array; the inversion identifies either −26.6° (T1) or 45° (T2) as the source bearing and often obtains approximately correct values for the corresponding r, ϕ, and v. The inversion does not converge to an incorrect bearing even when the sound level received on the array from the two sources is equivalent. If one of the sources is louder than the other, then r, ϕ, and v can also be well approximated by a single SDRC inversion.

B. Four well-separated targets

For the second example, a series of SDRC inversions and notch filters are applied to the field produced by four sources (T1–T4), which are well separated in bearing, to obtain estimates of the source locations and trajectories. Examples of 10° notch filters at 50 and 250 Hz are shown in Fig. 3.[24] The source configuration used to create the data are listed in Table II, and the locations and motion of the sources over the 3-min interval are illustrated in Fig. 4. Each source has a unique source spectra.

One way to examine the progress of the iterative, invert-and-filter method is to view scatter plots of the cost function E versus the individual parameters for all states visited in each SDRC inversion.[1] Envelopes of the scatter plots,[2] which essentially trace the minimum values of E found for each parameter, are shown in Figs. 5–9. The line representations of the scatter plots include on the order of 10 000 model realizations.

TABLE II. Characteristics of the four sources (T1–T4) for the synthetic data described in Sec. III B. The last two columns list the bounds on the parameters for the inversions.

Parameters	T1	T2	T3	T4	Min	Max
z_s (m)	30	20	6	40	1	85
r_0 (km)	2.828	5.099	5.000	6.325	0.1	10
θ (deg)	45	11.3	−36.9	−71.6	−90	90
ϕ (deg)	45	0	180	90	0	360
v (m/s)	2.0	2.0	2.0	2.0	0	10
SL (dB)	125	130	140	125		

Figure 5 contains plots of E versus initial source bearing θ for each of the four, successive, SDRC inversions and illustrates how application of the invert-and-filter method systematically obtains all four source bearings. The first inversion, performed on the original data, finds a minimum value of E at θ=11°, the initial bearing of T2, as depicted in Fig. 5(a); a second deep minimum is also visible at θ=−37°, the initial bearing of T3. The results of the second inversion performed after notch filters remove T2, shown in Fig. 5(b), yield a well-defined minimum of the E at θ=−37° (T3). Figure 5(c) shows how the third inversion (after T2 and T3 have been removed) results in θ=45° (T1). The plot of E vs θ for the fourth and final inversion, Fig. 5(d), reveals a sharp minimum at the initial bearing of T4, θ=−72°.

Figures 6–9 show the inversion results for the remaining four source parameters obtained by the four, successive inversions detailed Fig. 5. The width of the minima indicates the relative uncertainty in the inversion results: the wider the valley around the minimum, the more uncertain the estimate obtained by the inversion. The vertical dashed lines show the correct values, except in Fig. 6(c) where the correct answer is

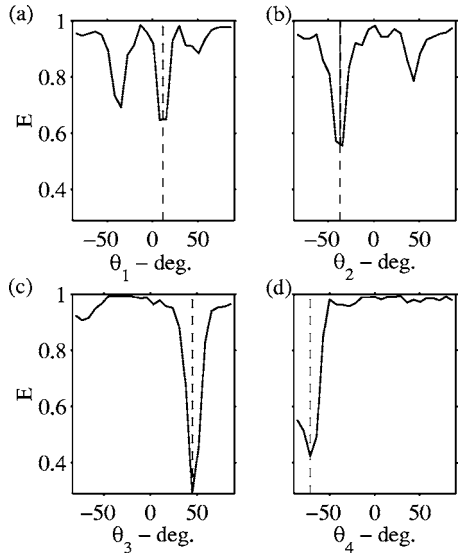

FIG. 5. Distribution envelopes of bearing θ vs cost function E for the four, successive, SDRC inversions in Sec. III B. The vertical dashed lines show correct bearings for (a) T2, (b) T3, (c) T1, and (d) T4.

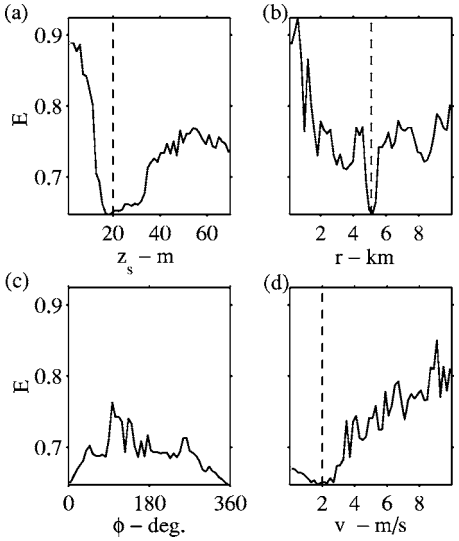

FIG. 6. Distribution envelopes of (a) z_s, (b) r, (c) ϕ, and (d) v vs cost function E for the first SDRC inversion in Sec. III B on the original four source data. The vertical dashed lines are the correct values for source T2.

$\phi=0°=360°$. In Fig. 6, all four source parameters for T2 are well approximated by the first SDRC inversion on the original four-source data. Figure 7 shows the results of the second inversion on data modified by notch filters to remove 10° about $\theta=11°$, the initial bearing of T2, in which good estimates are obtained for r, ϕ, and v of T3 but not for z_s. The correct z_s for T3 is 6 m, and as has been stated in Refs. 1 and 2, it is very difficult to find a shallow source depth accurately. Figures 8 and 9 show similar results: the source parameters for T1 and T4 are well approximated by the third and fourth SDRC inversions based on data modified by notch filters. Thus, the four sources have been localized, with the exception of one source depth, and tracked over the 3-min time interval by successive application of the single-source, SDRC inversion method and notch filters.

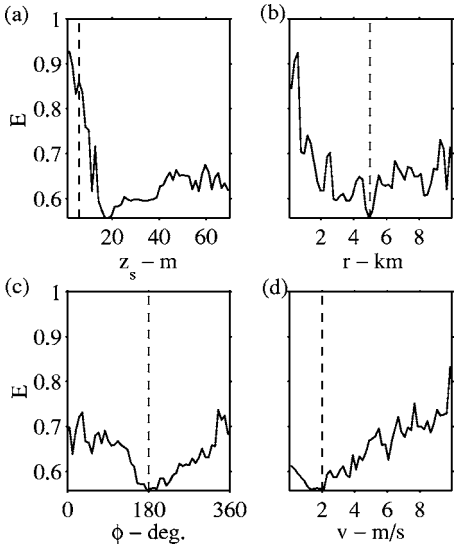

FIG. 7. Distribution envelopes of (a) z_s, (b) r, (c) ϕ, and (d) v vs cost function E for the second SDRC inversion in Sec. III B after T2 has been filtered out. The vertical dashed lines are the correct values for source T3.

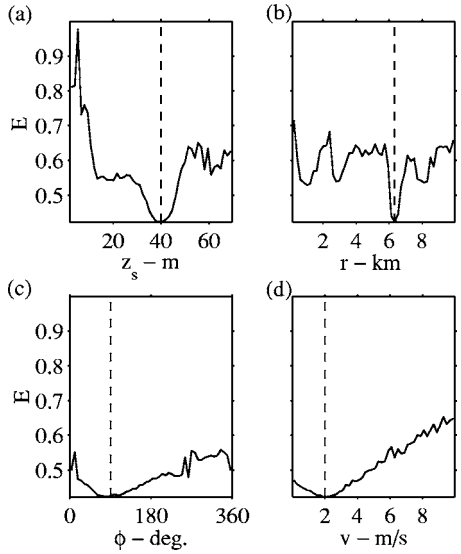

FIG. 8. Distribution envelopes of (a) z_s, (b) r, (c) ϕ, and (d) v vs cost function E for the third SDRC inversion in Sec. III B after T2 and T3 have been removed by notch filters. The vertical dashed lines are the correct values for source T1.

C. Ten targets

The iterative invert-and-filter approach is applied to data from ten, concurrent sources (T1–T10), designed to simulate a noisy, high-traffic area of the ocean, to explore how many sources can be localized and tracked with this approach. The bearing identification and notch filters are applied as in Sec. III B. In addition, passband filters are constructed around each identified bearing and applied to the data. The resulting filtered data sets are used in SDRC inversions to localize and track the sources. The positions of the sources during a 3 -min time interval are illustrated in Fig. 10. Five of the ten sources (T2, T6–T9) are loud surface ships (with $z_s \leqslant 10$m) traveling in parallel directions ($\phi=135°$ or 315°). The remaining five sources are located at a wide variety of depths

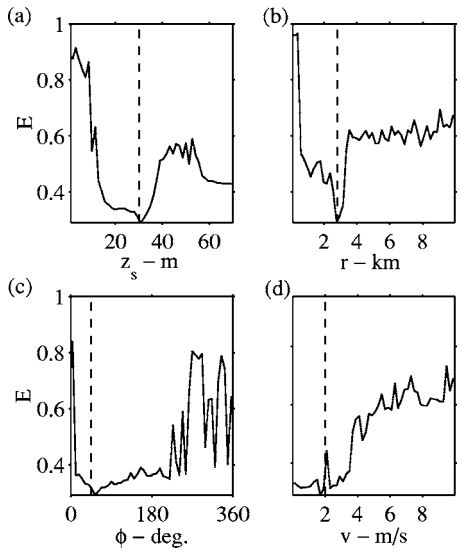

FIG. 9. Distribution envelopes of (a) z_s, (b) r, (c) ϕ, and (d) v vs cost function E for the fourth and final SDRC inversion in Sec. III B after T1, T2, and T3 have been removed by notch filters. The vertical dashed lines are the correct values for source T4.

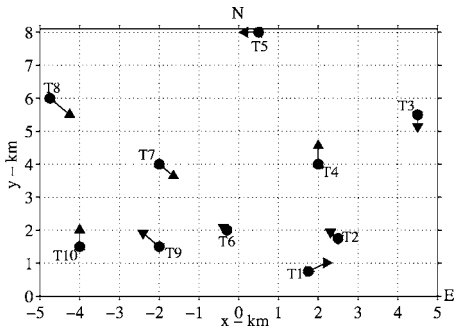

FIG. 10. Source configuration the ten sources (T1–T10) used in Sec. III C.

and ranges, with T5 being the quietest source and furthest from the array. In addition, a Gaussian noise background is added such that the signal-to-noise ratio with respect to the quietest source, T5, is 3 dB. The same frequencies, array configuration, and time sequences are used in these inversions as in the previous examples.

To follow the performance of the invert-and-filter method, envelopes of the distribution of the initial source bearing θ versus the cost function E for the successive SDRC inversions are plotted in Fig. 11. The dashed line in each plot is the initial bearing of the source shown in Fig. 10 that is closest to the bearing associated with the minimum value of

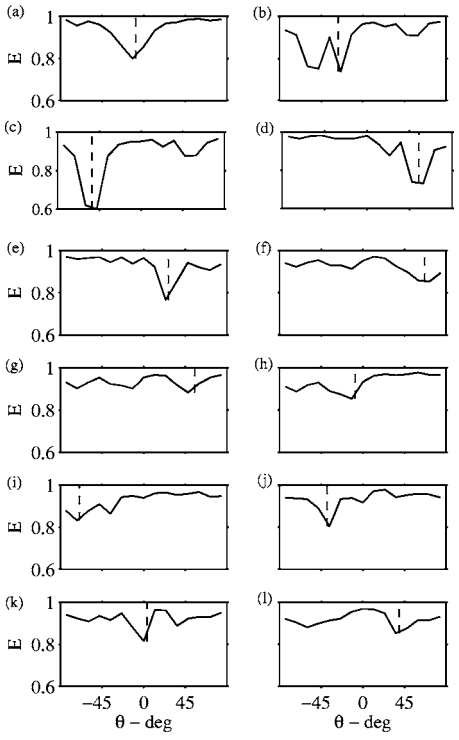

FIG. 11. Envelopes of the distributions of initial source bearing θ vs cost function E for the inversions described in Sec. III C. The dashed line in each plot is the initial bearing of the source shown in Fig. 10 that is closest to the value corresponding to the minimum E. In (a), the first SDRC inversion performed on the ten-source data finds the minimum values of E to be at $\theta=-11°$, close to the bearing of source T6. Each inversion (b)–(l) is performed using data modified by notch filters that remove one additional source. The source bearings identified by this method are (a) T6, (b) T7, (c) T9, (d) T2, (e) T4, (f) T1, (g) T2, (h) T6, (i) T10, (j) T8, (k) T5, (l) T3. The bearing of T2 and T6 are found twice because the initial notch filters are not wide enough to remove large sidelobes associated with T2 and T6.

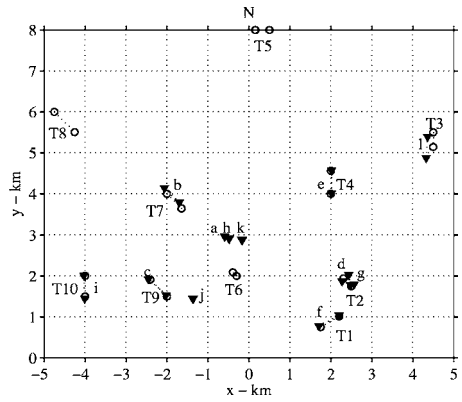

FIG. 12. Source locations resulting from inversions performed on data filtered about the bearings obtained in Fig. 11. Triangles mark the initial and final positions. The corresponding letters (a)–(l) label which filtered data set produced which trajectory. The actual beginning and ending source positions are shown as open circles and labeled T1–T10 as in Fig. 10.

E found in that inversion. In between the inversions, notch filters are created that remove 10° about each bearing identified thus far, and the filters are applied to the original data. Thus, the nth inversion uses data modified by notch filters with $n-1$ angular sectors removed. The first SDRC inversion performed on the ten-source data finds the minimum values of E at $\theta=-11°$, close to the initial bearing of source T6, as shown in Fig. 11(a). Figures 11(b)–11(f) display the results of the next five inversions that obtain good estimates for the bearings of sources (b) T7, (c) T9, (d) T2, (e) T4, and (f) T1. The loudest sources' bearings are found first. The next two inversion, shown in Figs. 11(g) and 11(h), yield bearings that are close to the values already found for T2 and T6 indicating that the 10° window removed by the notch filter is not sufficiently large to remove the main sidelobes of T2 and T6. Additional notch filters are used to extend the nulled angular sector about the estimated bearings. The remaining four inversions, Figs. 11(i)–11(l), find a miniumum near the initial bearings of (i) T10, (j) T8, (k) T5, and (l) T3. Thus it appears that all ten source bearings have been obtained using the invert-and-filter approach.

The next task is to obtain estimates of depth, range, and trajectory for each source whose bearing is identified by the invert-and-filter technique. First, separate filters are designed to pass 15° about each θ obtained by the 12 inversions displayed in Fig. 11. Next, the filters are applied to the original data, and the twelve filtered data sets, labeled (a)–(l) in accordance with Fig. 11, are processed in SDRC inversions to obtain estimates of z_s, r, ϕ, and v for each source. All twelve data sets are used, even though two of them are essentially duplicates because in realistic applications the true source bearings are not known.

A plot of the source locations over the 3-min time interval as obtained by the 12 inversions are plotted in Fig. 12, with triangles at the beginning and end locations, and are labeled (a)–(l) to indicate which of the filtered data sets yield which source parameters. The beginning and ending locations of the original, ten sources are shown as open circles. The HLA is located at the origin and extends along the $+x$ axis. From this plot, it is seen that the inversion using data filtered to pass 15° about the bearing identified in Fig. 11(f)

TABLE III. Source depths for the true source configuration in Fig. 10 and those obtained by the inversions in Figs. 12, 13(b), and 14(b). Inverted source depths are not listed for T5 and T8 because they are not localized by the inversion method.

Source	True	Inverted	B1	C1
T1	30	33	33	31
T2	6	16	14	14
T3	50	49	66	49
T4	20	19	27	20
T5	40	*X*	*X*	*X*
T6	6	34	38	33
T7	6	27	11	14
T8	10	*X*	*X*	*X*
T9	10	16	12	12
T10	15	14	5	16

of $\theta=66°$ obtains good estimates for the range, course angle, and speed of T1. Similarly, inversions based on filtered data sets (d) and (g) both yield good values for T2, confirming the idea that the bearing obtained in inversion (g) converges to a portion of the signal from T2 that is not removed by notching out a 10° angular sector about the bearing obtained by inversion (d). T3 is found using filtered data set (l), T4 by (e), T7 by (b), T9 by (c), and T10 by (i). Sources T5 and T8 are not identified using any of the filtered data sets.

Four of the 12 inversions did not converge accurately to correct source locations. Inversions (a) and (f) have the same bearing as T6, which is the loudest source, but the range is incorrect. This error occurs because T6 is the slowest of all the sources, $v=0.7$ m/s, and is moving too slowly for the range to be adequately determined by this cost function. Although the range estimates from inversions (a) and (f) are too large, the bearing, course angle and slow speed are found correctly. The other two inversions with poor results correspond to Figs. 11(j) and 11(k), even though the estimated bearings are close to the bearings of T8 and T5. The probable reasons for the inability to localize T5 and T8 are (1) the larger distance from the HLA and (2) the proximity to the loudest source T6. In addition, the results labeled (j) and (k) have very slow speeds similar to (a) and (f).

The source property that is not represented in Fig. 12 is the source depth. Table III lists the correct source depths and those obtained by the inversions performed on the filtered data sets. Although there is difficulty in obtaining accurate estimates for very shallow source depths, $z_s<10$ m, the remaining source depth estimates are within a few meters of the correct values.

The error in the inversions (j) and (k) and the inability to isolate the bearings of T5 and T8 demonstrate the limits of the invert-and-filter approach. At some point, after many angular sectors have been removed by the notch filters, the inversion can converge on either sidelobes of louder sources or on some feature of the interference between sidelobes of different sources. Thus, remaining sidelobe features can mask quieter sources. To locate quiet targets, a better way of removing the entire signal of the loud sources is required.

D. Environmental mismatch

In the previous examples, the properties of the shallow ocean environment are assumed to be known exactly. In cases where an approximately correct environment is used, then inversion such as those in Sec. III C generally yield reasonable source locations and trajectories. If the environmental information is very incorrect, it is still possible to obtain bearings of the sources with the invert-and-filter method. In the case of corrupt environmental information, a SDRC inversion, on data filtered to pass a loud source, in which both the source and environmental parameters are allowed to vary yields a modified description of the environment that can then be used to get improved estimates of the remaining sources' locations.

To examine the effect of environmental mismatch on the source localization process, two environments, listed as "B" and "C" in Table V, are considered. Environment B corresponds to a softer sediment with a ratio of water to sediment sound speed rc_1 less than one, while C represents a harder sediment. The process in Sec. III C is repeated twice more with the incorrect environments held fixed. In both cases, the source-bearing identification and source-removal procedure yields results equivalent to those in Fig. 11. The ability of the inversion to obtain correct source bearings with incorrect environments is evidence of the lack of coupling between the source bearing and the environment.[1] In addition, the matrix filters are based on plane-wave replica vectors and thus are independent of the assumed environment.

Once approximate source bearings have been estimated, data filtered to about each bearing are used in separate SDRC inversions for source parameters holding the incorrect environments fixed. In most instances, fairly good estimates are obtained for the course angle and speed but poorer estimates are obtained for the range and the depths. The ability of the inversions to determine relatively good estimates of ϕ and v independent of the environment is expected because they are not as significantly coupled to the environment as are z_s and r_0.

The inversion estimates are improved if a modified environment is used. The properties of the incorrect environment are allowed to vary along with the source parameters in the inversion based on data filtered around the source at −53°, a loud surface ship (T9), because it was the second bearing identified. (In general, the first bearing could be used, but in this case T6, the loudest source, is moving too slow to yield good results, as described in Sec. III C.) The bounds on the environmental parameters used in the inversion are listed in Table IV. The estimates of the environmental properties obtained by SDRC inversions on the loud source T2 are listed in Table V as B1 and C1 and are referred to hereafter as the modified environments. The estimates obtained for the most sensitive feature, rc_1, are closer to the correct value. The inversions on the filtered data sets for the other sources are performed again holding the modified environments fixed, and the resulting source locations and trajectories are shown in Fig. 13(b) for environment B1 and Fig. 14(b) for C1. The source depths are listed in Table III under B1 and C1.

TABLE IV. Environment used to generate the simulated data set in Sec. III is given in the column labeled "True." The last two columns contain the bounds on the nine environmental parameters varied in the inversions in Sec. III D. The ratio of the sound speed across interface i is labeled as rc_i; gc_i is the gradient of the sound speed in layer i.

Parameters	True	Min	Max
h_w (m)	115.3	112	118
h_1 (m)	27.1	25	50
ρ_1 (g/cm^3)	1.54	1.0	2.5
rc_1	1.038	0.98	1.30
gc_1 (1/s)	2.103	0	5
c_1 (m/s)	1516		
c_2 (m/s)	1573		
α_1 (dB/m/kHz)	0.15	0.0	0.5
ρ_{hsp} (g/cm^3)	1.85	1.5	2.5
rc_{hsp}	1.113	1.0	1.5
c_{hsp} (m/s)	1751		
α_{hsp} (dB/m/kHz)	0.2	0.05	0.8

The source locations and trajectories produced when the modified environments are used are very similar to those obtained using the correct environment. Thus, the overall invert-and-filter approach to obtaining multiple source locations and trajectories can be applied in cases where little is known about the seafloor.

IV. CONCLUSIONS

The iterative invert-and-filter technique has been tested on several synthetic cases to locate and track multiple, concurrent targets in both known and uncertain shallow ocean environments. The inherently single-source, SDRC inversion algorithm successfully identifies the bearing of the strongest source when applied to simulated, broadband, HLA data.

When a passband filter designed about the identified bearing is applied to the data, the resulting filtered data are processed in a SDRC inversion to obtain good estimates for the source range, course angle, speed, and source depth with two exceptions. (1) Incorrect range estimates are often found for source speeds less than 1 m/s using the the cost function specified in Eq. (1), which includes a summation over time sequences. (2) It is difficult to obtain accurate estimates for shallow source depths, i.e., less than 10 m.

Stop band or notch filters are also designed about the identified bearing and applied to the data effectively removing the sound originating from that angular sector. A SDRC inversion on this filtered data yields the bearing of the next loudest source. Additional applications of filters and inver-

TABLE V. Two test environments, B and C, used in Figs. 13(a) and 14(a), respectively. Two modified environments, B1 and C1, obtained by a SDRC inversion on a loud source, that are used for Figs. 13(b) and 14(b), respectively.

Parameters	B	C	B1	C1
h_w (m)	115	115	117.5	114
h_1 (m)	25	30	33	23
ρ_1 (g/cm^3)	1.4	1.7	1.86	1.34
rc_1	0.99	1.13	1.023	1.035
gc_1 (1/s)	2	2.8	3.03	4.65
c_1 (m/s)	1450	1650	1493	1511
c_2 (m/s)	1500	1735	1595	1617
α_1 (dB/m/kHz)	0.1	0.16	0.24	0.23
ρ_{hsp} (g/cm^3)	1.67	2.0	1.58	2.13
rc_{hsp}	1.117	1.110	1.218	1.11
c_{hsp} (m/s)	1675	1925	1942	1970
α_{hsp} (dB/m/kHz)	0.18	0.22	0.31	0.18

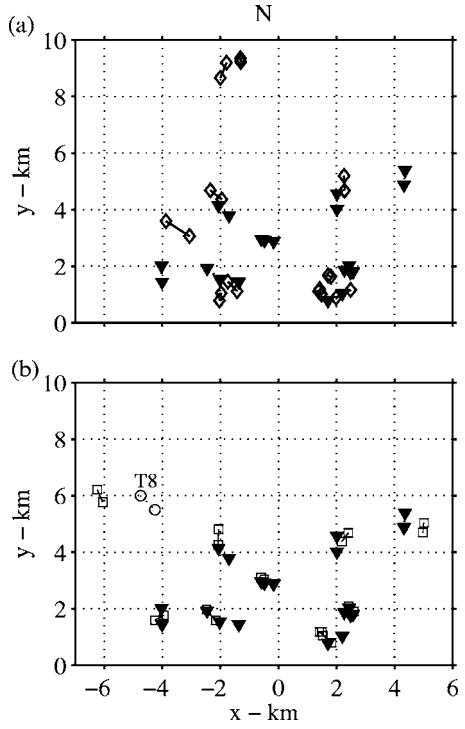

FIG. 13. Comparison of source locations obtained using correct environment (closed triangles, the same as in Fig. 12) in (a) to those found with environment B (open diamonds) and in (b) to those found using the modified environment B1 (open squares) obtained from a loud source.

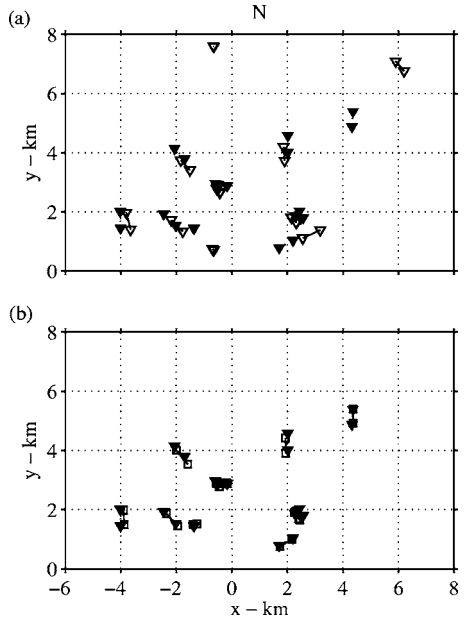

FIG. 14. Similar to Fig. 13 except environment C is used in (a) and modified environment C1 is used in (b).

sions reveal additional source bearings. If the notch filter is not sufficiently large, the inversion may converge on a main sidelobe of a source that has been previously identified. In such cases, the subsequent inversion on the pass-filtered data converges to the same location as a previous source indicating a duplication of source bearing. While it is possible for a source to be too quiet to be detected or for it to be masked by sidelobes or interference patterns remaining after other sources are removed by the filters, in most cases, many sources can be accurately localized with the invert-and-filter technique.

The performance of the invert-and-filter scheme in the presence of environmental mismatch has been investigated. Incorrect environmental information does not impede the bearing-identification and source-removal procedure. In cases of large environmental mismatch, the estimates of source range and depth can be improved when a modified environment, obtained from an inversion based on filtered data corresponding to a loud source, is used.

It is possible that filters based on the environment, instead of on the plane-wave assumption, might improve the effectiveness of the notch filter.[25] However, the sensitivity of such filters to environmental mismatch could be substantial and needs to be investigated.

ACKNOWLEDGMENTS

This work was supported by the Office of Naval Research. The author wishes to acknowledge that Dr. Craig S. MacInnes introduced her to the passband matrix filters and that Dr. Gary Wilson first suggested that the inversion method be applied directly to multisource problems. The author also wishes to thank Dr. David Knobles and Dr. Robert Koch, Dr. Steven Stotts, and Eric Ridderman for their helpful comments and discussions regarding this work. In addition, gratitude is expressed to the reviewers who made valuable suggestions and comments.

[1]T. B. Neilsen, "An iterative implementation of rotated coordinates for inverse problems," J. Acoust. Soc. Am. **113**, 2574–2586 (2003).
[2]T. B. Neilsen and D. P. Knobles, "Geoacoustic inversion of range-dependent data with added Gaussian noise," IEEE J. Ocean. Eng. **28**, 446–453 (2003).
[3]C. S. MacInnes, "Source localization using subspace estimation and spatial filtering," submitted IEEE J. Ocean. Eng. (submitted).
[4]H. Cox, R. M. Zeskind, and M. M. Owen, "Robust adaptive beamforming," IEEE Trans. Acoust., Speech, Signal Process. **35**, 1365–1376 (1987).
[5]A. Tolstoy, *Matched Field Processing for Underwater Acoustics* (World Scientific, Englewood Cliffs, NJ, 1993).
[6]E. K. Westwood, "Broadband matched-field source localization," J. Acoust. Soc. Am. **91**, 2777–2789 (1992).
[7]A. B. Baggeroer, W. A. Kuperman, and P. N. Mikhalevsky, "An overview of matched-field methods in ocean acoustics," IEEE J. Ocean. Eng. **18**, 401–424 (1993).
[8]*Full Field Inversion Methods in Ocean and Seismo-acoustics*, edited by O. Diachok, A. Caiti, P. Gerstoft, and H. Schmidt (Kluwer Academic, Dordrecht, 1995).
[9]A. Tolstoy, N. R. Chapman, and G. Brooke, "Workshop '97: Benchmarking for geoacoustic inversion in shallow water," J. Comput. Acoust. **6**, 135–150 (1998).
[10]N. R. Chapman, S. Chin-Bing, D. King, and R. B. Evans, "Benchmarking geoacoustic inversion methods for range-dependent waveguides," Phys. Lett. A **28**, 320–330 (2000).
[11]S. E. Dosso, "Quantifying uncertainty in geoacoustic inversion. I. A fast Gibbs sampler approach," J. Acoust. Soc. Am. **111**, 129–142 (2002).
[12]S. E. Dosso and P. L. Nielsen, "Quantifying uncertainty in geoacoustic inversion. II. Application to broadband, shallow-water data," J. Acoust. Soc. Am. **111**, 143–159 (2002).
[13]Z. Michalopoulou and U. Ghosh-Dastidar, "Tabu for matched-field source localization and geoacoustic inversion," J. Acoust. Soc. Am. **111**, 135–145 (2004).
[14]M. D. Collins and W. A. Kuperman, "Focalization: Environmental focusing and source localization," J. Acoust. Soc. Am. **90**, 1410–1422 (1991).
[15]E. K. Westwood, C. T. Tindle, and N. R. Chapman, "A normal mode model for acousto-elastic environments," J. Acoust. Soc. Am. **100**, 3631–3645 (1996).
[16]M. D. Collins and L. Fishman, "Efficient navigation of parameter landscapes," J. Acoust. Soc. Am. **98**, 1637–1644 (1995).
[17]W. H. Press, A. Teukolsky, W. T. Vetterling, and B. P. Flannery, *Numerical Recipes in FORTRAN: The Art of Scientific Computing* (Cambridge University Press, Cambridge, 1992), Sec. 7.8.
[18]H. Szu and R. Hartley, "Fast simuated annealing," Phys. Lett. A **122**, 157–162 (1987).
[19]R. J. Vaccaro and B. F. Harrison, "Optimal matrix filter design," IEEE Trans. Signal Process. **44**, 705–709 (1996).
[20]R. J. Vaccaro and B. F. Harrison, "Matrix filters for passive SONAR," in Proceedings of the ICASSP 2001 International Conference on Acoustics, Speech and Signal Processing, Salt Lake City, UT, May 2001.
[21]G. H. Golub and C. F. Van Loan, *Matrix Computations*, 3rd ed. (Johns Hopkins University Press, Baltimore, 1996).
[22]S. A. Stotts, "A robust spatial filtering technique for multisource localization and geoacoustic inversion" J. Acoust. Soc. Am., **118**, 139–162 (2005).
[23]E. A. Ridderman and D. Knobles, University of Texas at Austin (private communication).
[24]For bearings close to endfire of the array, the matrix filters have large sidelobes for frequencies not well sampled by the array elements because the spacing between array elements is greater than one half the wavelength.
[25]R. J. Vaccaro, A. Chetri, and B. F. Harrison, "Matrix filter design for passive sonar interference suppression," J. Acoust. Soc. Am. **115**, 3010–3020 (2004).